HHS Public Access

Author manuscript

Nat Struct Mol Biol. Author manuscript; available in PMC 2009 October 05.

Published in final edited form as:

Nat Struct Mol Biol. 2009 March ; 16(3): 325–333. doi:10.1038/nsmb.1555.

Helix sliding in the stalk coiled coil of dynein couples ATPase and microtubule binding

Takahide Kon[1], **Kenji Imamula**[1], **Anthony J. Roberts**[2], **Reiko Ohkura**[1], **Peter J. Knight**[2], **I. R. Gibbons**[3], **Stan A. Burgess**[2], and **Kazuo Sutoh**[1]

[1]Department of Life Sciences, Graduate School of Arts and Sciences, University of Tokyo, Komaba 3-8-1, Tokyo 153-8902, Japan.

[2]Astbury Centre for Structural Molecular Biology and Institute of Molecular and Cellular Biology, University of Leeds, Leeds LS2 9JT, U.K.

[3]Molecular and Cell Biology Department, University of California, Berkeley, California 94720, USA.

Abstract

Coupling between ATPase and track-binding sites is essential for molecular motors to move along cytoskeletal tracks. In dynein, these sites are separated by a long coiled-coil stalk which must mediate communication between them, yet the underlying mechanism remains unclear. Here we show that changes in registration between the two helices of the coiled coil can perform this function. We locked the coiled coil at three specific registrations using oxidation to disulfides of paired cysteine residues introduced into the two helices. These trapped ATPase activity either in a microtubule-independent high or low state, and microtubule-binding activity either in an ATP-insensitive strong or weak state, depending on the registry of the coiled coil. Our results provide direct evidence that dynein uses sliding between the two helices of the stalk to couple ATPase and microtubule-binding activities during its mechanochemical cycle.

INTRODUCTION

Dynein is an enormous motor complex that consumes ATP to move along microtubules (MT) toward their minus ends1,2. This motile activity is critical for many cellular processes within eukaryotic cells, including the beating motions of cilia and flagella, mitosis, cell migration and the retrograde transport of various vesicles and organelles3–5. When compared to the other cytoskeletal motor proteins, myosin and kinesin, much less is known about the molecular mechanism of dynein action.

Correspondence should be addressed to K.S. (sutoh@bio.c.u-tokyo.ac.jp).

AUTHOR CONTRIBUTIONS

T.K., I.R.G and K.S. designed the study; T.K., K.I. and R.O. performed the biochemical experiments; A.J.R., P.J.K. and S.A.B. performed the EM analyses; K.S. supervised the study; T.K. wrote the first draft of the manuscript and all authors contributed to the preparation of the final version.

The dynein complex is composed of one to three heavy chains (each >500 kDa) and a number of smaller associated polypeptides3,6. Among them, the heavy chain, belonging to the AAA^+ superfamily of mechanochemical enzymes7, is responsible for the motile activity of dynein8,9. The heavy chain consists of four structurally and functionally distinct units: head, tail, stalk, and MT-binding (MTBD) domains (Fig. 1a, b). The head contains six tandemly linked AAA^+ modules (AAA1 to AAA6) arranged in a ring-shaped structure10 that is a common feature of AAA^+ proteins11. The first four AAA^+ modules can bind ATP and/or ADP12, with AAA1 being the principal ATPase site and AAA3 also playing an important role in motor activity13–16. From this head, the tail and stalk domains emerge as long, slender structures17,18. The tail functions in multimerization of the heavy chains and binding to the cargoes19, whereas the stalk, a predicted antiparallel α-helical coiled coil, has the globular MTBD at its tip20,21.

A critical mechanism underlying the motile activity of cytoskeletal motor proteins is precise coupling between ATPase and track-binding activities. During a mechanochemical cycle, ATPase steps regulate the affinity for the track, allowing the motor to detach or attach, while track binding activates one of the ATPase steps to ensure tight coordination of the ATPase and motile activities22. In myosin and kinesin, both ATPase and track-binding sites are involved in a globular head domain and located relatively close to each other23, which allows them to communicate directly. In dynein, by contrast, the ATP-hydrolyzing AAA^+ head and MTBD are well separated by the 10–15 nm stalk coiled coil20 (Fig. 1b). This unique structural design of dynein raises a key question of how the motor carries out long-range two-way communication through the stalk coiled coil to couple the two functional activities.

There are several clues to the mechanism of stalk-mediated two-way communication. Since the coiled coil is potentially a stable fold and, as observed by electron microscopy (EM), the stalk remains intact at different stages of the ATPase cycle17, it has been speculated that changes in helix-helix interactions along the stalk coiled coil could transmit structural information between head and MTBD20,24,25. Consistent with this, an EM study showed that the structural flexibility of the stalk alters without changing its length, depending on the nucleotide-bound state of dynein18. More recently, Gibbons *et al.*26 sought to identify the optimal coiled-coil register of the stalk using a series of recombinant MTBD together with adjacent stalk whose registry was fixed by fusion onto a stable coiled-coil base. The fusion constructs whose stalk is expected to be fixed in one registry show high binding affinities for MT, while those in other registries examined display much lower affinities. Based on the results together with a homology-based structural model of the stalk, the authors have hypothesized that small amounts of sliding between the two helices of the stalk play a role in the communication.

These studies, especially the helix-sliding hypothesis, have provided valuable insights into conformational changes in the stalk domain. However, the predicted conformational changes need to be tested in functional dynein. Furthermore, the relationships among the stalk conformation, ATPase, and MT-binding activities should be determined to reveal how the stalk-mediated communication is achieved in dynein. Here, we have carried out such a study by means of a disulfide cross-linking approach using the 380-kDa motor domain of the

Dictyostelium discoideum cytoplasmic dynein, which retains full motor activities8. To reversibly lock the stalk of the motor domain into particular registries, we used disulfide bonds between pairs of cysteine residues engineered into the two helices of the stalk coiled coil. By determining motor properties of the resultant dynein, we show that locking the stalk coiled-coil registry uncouples ATPase and MT-binding activities. Furthermore, we find that ATPase activity is trapped in either a 'high' or 'low' state, and MT-binding activity is fixed in either a 'strong' or 'weak' state, depending on the locked registry of the stalk coiled coil. Collectively, our results provide direct evidence that dynein uses sliding between the two helices of the stalk coiled coil to couple ATPase and MT-binding activities during its mechanochemical cycle.

RESULTS

Design of double-Cys mutants for locking the stalk registry

The purpose of the present study was to elucidate how the stalk, a predicted antiparallel α-helical coiled coil, mediates the two-way communication between the ATP-hydrolyzing AAA^+ head and the MTBD in the dynein heavy chain. A current hypothesis is that small amounts of sliding between the two helices of the stalk coiled coil, causing a shift in the coiled-coil register, play a role in this communication26. We thus employed a disulfide cross-linking approach to fix a particular registry of the stalk coiled coil and then examined the effects on ATPase and MT-binding activities. To achieve this, we replaced two residues in the stalk coiled coil with cysteines: one residue located in the outward helix (CC1) and another residue in the return helix (CC2) (Fig. 1). We used the monomeric 380-kDa motor domain of the *Dictyostelium discoideum* cytoplasmic dynein heavy chain fused at its N-terminus with His_6-FLAG-EGFP tag (HFG380; Fig. 1a), which consists of the N-terminal truncated tail domain and entire head, stalk, and MTBD domains, and also retains dynein's motor activities16. Although HFG380 contains 35 endogenous cysteine residues, its predicted stalk coiled-coil region (CC1: residues 3248–3365; CC2: residues 3492–3632) does not include any cysteine residues. Using HFG380 dynein as wild type, we created three double-Cys mutants: L3339C Q3510C, Q3340C I3513C, and L3339C I3517C (Fig. 1b, c). These mutants were designed based on a homology-based structural model for the stalk coiled coil26, which predicts that L3339 or Q3340 located in CC1 forms a hydrophobic pair with Q3510, I3513, or I3517 in CC2. When a disulfide bond between the two introduced Cys residues is formed by oxidation, the alignment in the stalk coiled coil of L3339C Q3510C, Q3340C I3513C, and L3339C I3517C is expected to be fixed in one of three registries, referred to as +β, α, and −β, respectively (Fig. 1d). With reference to the α registry, +β and −β fixations cause a half-heptad shift (4 or 3 residues respectively) in alignment in opposite directions. Hereafter, we refer to L3339C Q3510C, Q3340C I3513C, and L3339C I3517C as +β, α, and −β mutants, respectively. In the present study, we did not examine other possible stalk registries or non-register positions, mainly because several of Cys substitutions along the stalk, other than those described above, had profound effects on ATPase activity even without oxidation (data not shown).

Disulfide cross-linking within the stalk coiled coil

Disulfide bond formation within the stalk coiled coil was assayed by an electrophoretic mobility shift test. Because the molecular mass of the dynein motor domain is too high to detect the shift, the stalk domain was cleaved from the motor before electrophoresis. To this end, we engineered HFG380P dynein in which two PreScission protease cleavage sites were created for protease-mediated excision of an 83-kDa fragment containing the stalk domain (Fig. 2a). Creating these sites did not substantially affect motor activity as judged by MT-activated ATPase properties of HFG380P (basal, k_{cat}, and K_m(MT) values of 9.3 ± 0.9 s^{-1}, 132.0 ± 2.7 s^{-1}, and 18.4 ± 0.7 μM, respectively). The oxidized or reduced forms of the double-Cys mutants of HFG380P were treated with the protease and then analyzed by SDS-PAGE under non-reducing conditions. The treatment produced three fragments, as expected (Fig. 2b). Among them, the ~80-kDa band was identified as the stalk fragment by immunoblotting with an anti-stalk antibody (Fig. 2c).

An oxidation-induced mobility shift of the ~80-kDa band was observed in all three double-Cys mutants (Fig. 2b, c). This shift is due to intramolecular disulfide cross-linking of the introduced Cys pair, because neither the wild type nor the five single-Cys mutants (L3339C, Q3340C, Q3510C, I3513C, and I3517C) showed the shift (Supplementary Fig. 1a). Based on Coomassie staining (Fig. 2b), cross-linking efficiencies in the three double-Cys mutants were estimated at ~70–90% after 5-min oxidation with ATP present.

We also performed similar cross-linking experiments in the presence of specific nucleotides together with the absence or presence of MT, each of which is expected to trap dynein in one of the intermediate states in its mechanochemical cycle. Although all three double-Cys mutants were finally cross-linked with high efficiencies (~60–90%), kinetics of the disulfide-bond formation varied depending on the nucleotide/MT conditions (Fig. 2d and Supplementary Fig. 1b). In the presence of excess ATP plus vanadate, dynein forms a stable ADP-Vi complex that mimics the ADP-Pi transition state27. Under the conditions, the +β mutant was cross-linked more rapidly than the other two mutants. In contrast, in the presence of excess ADP plus MT, the α mutant was cross-linked faster than the others. When oxidation was carried out in the presence of excess ADP alone as a control, all three double-Cys mutants were cross-linked so quickly that a maximum cross-linking occurred even at the earliest sampling point (0.5 min).

The oxidized double-Cys mutants of HFG380 were examined by negative-stain EM to determine the structural effects of stalk cross-linking. The molecules were monodisperse in each case (Supplementary Fig. 2a), confirming that the oxidizing treatment induced predominantly intramolecular, and not intermolecular, disulfide bond formation between the introduced Cys pair. Two-dimensional single-particle image processing revealed that there were no major differences in the architecture of the stalk and head domains between the oxidized double-Cys mutants and wild-type control (Supplementary Fig. 2b). Thus the three types of cross-linking within the stalk coiled coil have little impact on the global structure of the motor domain.

Effects of locking stalk registry on MT-binding and ATPase

We measured ATP-sensitive MT-binding activity and MT-activated ATPase activity of the cross-linked double-Cys mutants to examine the effects of locking the registry of the stalk coiled coil on two-way communication. We present here data on HFG380 and its mutants, although we obtained similar results for the ATPase activity of double-Cys mutants based on HFG380P and HFG380B2 (data not shown). The latter was used to examine the effects of stalk cross-linking on mechanochemical coupling as shown later.

MT-binding activity was first assayed before oxidation (*Untreated* in Fig. 3 and Table 1). As expected, in the absence of ATP, the wild type bound strongly to MT with a K_d of 0.66 ± 0.03 μM, whereas, in the presence of ATP, binding was weaker with a K_d of >10 μM. All three untreated double-Cys mutants also displayed near wild-type ATP-sensitive MT-binding activity with a K_d of <1 μM and >10 μM in the absence and presence of ATP, respectively. Oxidizing treatment inducing the disulfide cross-linking in the stalk coiled coil drastically altered the MT-binding properties of the double-Cys mutants without substantially affecting that of the wild-type control (*Oxidized* in Fig. 3 and Table 1). The oxidized +β and −β mutants showed weak binding to MT with a K_d of >10 μM. Conversely, the oxidized α mutant exhibited strong binding to MT with a K_d of <1 μM. Strikingly, the MT-binding activities of the oxidized mutants were independent of ATP. These novel properties of the mutants are attributed to disulfide cross-linking within the stalk coiled coil because the oxidizing treatment had no apparent effect on the ATP-sensitive MT-binding activity of all five single-Cys mutants (Supplementary Fig. 3). Thus, the MT-binding activity of the motor domain can be trapped in either an ATP-insensitive ‘strong’ or ‘weak’ state depending on the fixed registry of the stalk coiled coil.

ATPase measurements before oxidation (*Untreated* in Fig. 4 and Table 1) showed that the wild type has a basal rate of 4.9 ± 0.1 s^{-1}, and MT activated the rate up to ~25-fold with estimated k_{cat} and K_m(MT) values of 121.1 ± 4.9 s^{-1} and 32.1 ± 2.5 μM, respectively. Untreated +β and −β mutants exhibited near wild-type basal and MT-activated rates, whereas untreated α mutant showed 2–3-fold higher rates compared to the wild-type control. All three mutants had MT-activation properties near wild type: MT activated the ATPase rates up to 13–26-fold with K_m(MT) values of 15–41 μM, indicating that MT-binding information is properly transmitted between the MTBD and the ATP-hydrolyzing head in the untreated mutants.

Oxidation to lock the coiled coil registry with a disulfide bridge dramatically changed the ATPase properties of the double-Cys mutants without substantially affecting that of the wild-type control (*Oxidized* in Fig. 4 and Table 1). Even in the absence of MT, oxidized α and −β mutants showed high ATPase activity (128.4 ± 6.6 and 74.0 ± 2.1 s^{-1}, respectively) relatively close to the k_{cat} values for MT-activated ATPase in the corresponding untreated mutants (182.8 ± 4.8 and 116.4 ± 4.4 s^{-1}, respectively). Conversely, oxidized +β mutant had a basal rate (3.3 ± 0.1 s^{-1}) slightly lower than the untreated mutant (4.2 ± 0.3 s^{-1}). For all three oxidized mutants, MT had little further effect on the ATPase activity: oxidized α and −β were activated by only 1.2- and 1.5-fold, respectively, and oxidized +β stayed at a slow rate (k_{cat} value of 17.0 ± 0.6 s^{-1}). The remaining MT-induced activation can be attributed to

the minor (~10–30%) un-cross-linked population in the oxidized mutants, detected in the electrophoretic motility shift experiment (Fig. 2). These oxidation-induced changes in ATPase properties are due to disulfide cross-linking within the stalk coiled coil, because reduction following oxidation returned the activity of the mutants to their original levels (*Reduced* in Fig. 4 and Table 1), and furthermore, activities of all five single-Cys mutants were not substantially affected by the oxidizing treatment (Supplementary Fig. 4). Collectively, these results indicate that locking the stalk registry does not halt the ATPase cycle but fixes it in either an MT-independent 'high' or 'low' state depending on the registry.

To further confirm the dependence of ATPase activity on the registry of the stalk coiled coil, we created another series of mutants of the motor domain in which the MTBD (residues 3366–3491) was replaced by the stable antiparallel coiled coil from seryl-tRNA synthetase (SRS)26, to fix the registry of the stalk coiled coil near its distal end (Fig. 5a). By removing varying numbers of residues from the distal end of CC1, we shifted the alignment in the stalk coiled coil, yielding three mutants, +βCC, αCC, and −βCC, whose stalk registries are expected to be fixed in +β, α, and −β, respectively (Fig. 5b). As shown in Figure 5c, αCC and −βCC showed high ATPase rates (143.3 ± 11.2 and 143.2 ± 8.5 s^{-1}, respectively), comparable to the k_{cat} value for MT-activated ATPase in the wild-type motor domain. Conversely, +βCC exhibited a much lower ATPase rate (1.5 ± 0.1 s^{-1}), close to the wild-type basal rate. As expected, MT had no effect on ATPase activity of these MTBD-deficient mutants (data not shown). In summary, when the stalk registry is locked by two different methods, the results are consistent: α and −β registries communicate a high ATPase state to the AAA^+ head, whereas +β communicates a low ATPase state.

Effects of locking stalk registry on mechanochemical cycle

In addition to the modulation of MT binding at the MTBD, the ATPase cycle in the head also drives another, mechanically distinct, structural change, *i.e.*, swing-like motions of the tail domain, which has been proposed as a major contributor to force generation by dynein9,18,28. Previous studies have suggested that during an ATPase cycle, dynein performs a recovery-stroke and a subsequent powerstroke mainly by swinging its tail domain between pre-powerstroke and post-powerstroke positions relative to the head domain18,29 (Fig. 6a). Kinetic measurements have shown that the powerstroke transition, *i.e.*, the step in isolated dynein that is akin to the powerstroke along MT, is rate-limiting in the mechanochemical cycle in the absence of MT, and that MT accelerates this step30.

To determine whether locking the stalk registry, trapping dynein either in the high or low ATPase state, also influences the recovery-stroke and powerstroke processes, we monitored the ATPase cycle-driven tail motions in the double-Cys mutants by time-resolved fluorescence resonance energy transfer (FRET) measurements30. For this purpose, we used HFG380B2, which contains two fluorescent moieties, GFP fused to the tail and BFP inserted in the head, as FRET sensors for detecting tail motions (Fig. 6a), yet retains near-normal motor activities29. Like wild-type HFG380B230, double-Cys mutants of HFG380B2 showed the recovery-stroke and powerstroke transitions as monitored by a rapid increase and decrease, respectively, in FRET-induced GFP emission (Fig. 6b, c). The time courses

were well fitted to single exponentials except that the powerstroke transient in oxidized α and −β mutants required double exponentials. The apparent rate constants derived for the recovery-stroke transition (k_{obs}(post-pre)) and powerstroke transition (k_{obs}(pre-post)) are shown in Table 1. The amplitude of change in GFP emission varied depending on the mutant and the reduced/oxidized state, suggesting that the Cys substitutions and/or disulfide cross-linking within the stalk induce small conformational changes in the tail, head, or both, which could affect relative orientation and/or distance between the FRET sensors. However, before oxidation (*Untreated* in Fig. 6 and Table 1), all three double-Cys mutants had near-normal rate constants, k_{obs}(post-pre) of 156–163 s^{-1} and k_{obs}(pre-post) of 4.6–9.4 s^{-1}, which are close to the corresponding wild-type values (139.7 ± 8.4 s^{-1} and 4.9 ± 0.1 s^{-1}, respectively).

Oxidation to lock the stalk registry (*Oxidized* in Fig. 6 and Table 1) substantially accelerated the powerstroke transition in the high ATPase mutants (α and −β), but did not affect that in the low ATPase mutant (+β) and wild-type control. In oxidized α and −β mutants, the major phase (~80% in amplitude) showed a rapid powerstroke transition (k_{obs} of 47.5 ± 5.3 and 41.5 ± 1.3 s^{-1}, respectively) at least 5-fold faster than the corresponding untreated mutants. In addition, the transition contained a minor phase with a slower rate constant (~20% in amplitude; k_{obs} of 5.0 ± 0.7 and 3.9 ± 0.6 s^{-1}, respectively), close to the corresponding untreated value, which could be derived from the minor un-cross-linked population. In contrast, oxidation had little effect on the recovery-stroke transition in all three mutants as in the wild-type control. These results suggest that, as in the case of ATPase rate, shifts in stalk registry also regulate the tail motion at the powerstroke step in dynein's mechanochemical cycle.

DISCUSSION

The helix-sliding hypothesis passes direct tests

Our study has three major findings indicating that the sliding of the helices in the stalk coiled coil, causing a shift in the coiled-coil register, couples MT-binding and ATPase activities of the dynein motor domain. First, the relative positions of the two helices forming the stalk coiled coil appear to be inherently flexible and movable along its length in the range of at least one heptad repeat (Fig. 2). Second, inhibition of this mobility uncouples the MT-binding and ATPase activities of the motor domain (Fig. 3 and Fig. 4). Third, both MT-binding and ATPase activities of the motor domain are extremely sensitive to stalk registry, and thus the stalk cross-linking traps three allosteric states with distinct MT-binding/ATPase activities depending on the fixed stalk registry (Fig. 3 and Fig. 4). Collectively, these findings, together with results of the coiled-coil fusion experiments (Fig. 5), support the helix-sliding hypothesis26 and directly show that changes in the stalk registry between the three trapped states can act as a critical bidirectional switch for regulation of both MT-binding and ATPase activities, thereby coupling these two functional activities in the dynein motor domain. This predicts that MT binding at the MTBD or ATP binding/hydrolysis within the head domain serves as allosteric effectors inducing the change in the stalk registry to control ATPase or MT-binding activity at the other end of the stalk. However, from the dependence of the disulfide bond formation in the double Cys mutants on the nucleotide/MT

conditions (Fig. 2), we infer that these allosteric effectors do not fix the stalk coiled coil in a particular registry but shift the equilibrium between multiple registries. This notion is in line with the fact that several proteins, such as adenylate kinase and nitrogen regulatory protein C, use similar population-shift mechanisms for allosteric regulation31,32.

While this manuscript was under review, the crystal structure of the MTBD with a portion of the stalk was reported33. The structural analysis has shown that the stalk domain is indeed an antiparallel coiled coil.

A model for helix sliding in the mechanochemical mechanism

How do the changes in the stalk registry mediate the two-way communication during the mechanochemical cycle of dynein? In light of previous studies, stalk-mediated communication between the ATP-hydrolyzing head and the MTBD is required at least two stages in the mechanochemical cycle24. To explain its molecular mechanism, we present a simple model that correlates the changes in the stalk registry with steps in dynein's mechanochemical cycle (Fig. 7). In this model, we incorporate the two stalk registries, +β and α, together with current knowledge of dynein's mechanochemical cycle provided by previous reports29,30,34–36, as follows. (i) In the apo (no-nucleotide) state, the stalk coiled coil is in the α registry and dynein binds strongly to MT. (ii) Upon binding of ATP to the head domain, this information is transmitted to the MTBD, through a shift in the structural equilibrium of the stalk coiled coil from the α toward the +β registry, which induces dissociation of dynein from MT. (iii) Then, dynein performs a recovery stroke before hydrolysis of the bound ATP. (iv) After ATP hydrolysis and during phosphate and/or ADP releasing steps, dynein rebinds to MT and this information is communicated from the MTBD to the head, presumably through a reverse shift in the structural equilibrium of the stalk from the +β to the α registry, which accelerates the rate-limiting part of the ATPase cycle, *i.e.*, the product release step(s), coupled with the powerstroke of dynein. (v) After the product release, dynein returns to the initial apo state for the next cycle. We do not include the −β registry here because, unlike +β and α, this registry appears to represent a minor population in both of the two key intermediate states, as shown by its slower cross-linking kinetics (Fig. 2), and furthermore this model can work without the weak MT-binding/high ATPase state trapped by the −β registry. However, other more complex models that include all three registries, are also possible. For example, at step (*ii*), the dissociation of dynein from MT may be induced by a shift in the structural equilibrium of the stalk from the α to the −β registry instead of to the +β registry. In any case, however, our results are compatible only with models in which at step (*iv*), dynein sets its stalk in the +β and α registries just before and after the rebinding to MT, respectively, to perform the MT-based, ATPase cycle-dependent powerstroke. In addition, it should be noted that among the four potential ATP-binding/hydrolysis sites (AAA1–AAA4) in the head domain, our model focuses on the ATPase cycle at AAA1, because this is the primary site responsible for driving changes in MT-binding affinity, tail motions, and MT-based motility of cytoplasmic dynein16,29,36.

The changes in the stalk registry also might play a role in tension-dependent regulation of motor activity. Based on results of optical trapping experiments, it has been proposed that intramolecular tension alters stalk angle relative to the MTBD to modulate the MT-binding

affinity, which may be a key mechanism for two-headed dynein to move processively along MT37. Our results provide a possible mechanism for this process: the tension-induced stalk tilting could cause a change in the stalk registry between +β, α, and −β, which in turn modulates the MT-binding affinity of the MTBD. This model also predicts that the intramolecular tension could regulate dynein's ATPase cycle.

Helix sliding in other AAA+ proteins

In addition to dynein, relatively long coiled coils are included as functional units in some of the other AAA+ mechanochemical proteins, such as the molecular chaperones ClpB/Hsp104 and HslU, enhancer binding proteins NtrC1 and DctD, and AAA+ ATPases of eukaryotic and archaeal proteasomes38,39. These coiled coils are generally involved in recognition of substrate proteins and/or regulation of ATPase cycle-dependent mechanochemical activities, as in the case of the stalk coiled coil of dynein. Among them, the coiled coils of ClpB have features similar to that of dynein. ClpB has a set of coiled coils ~8.5 nm long in total that is located at a linker region between two AAA+ modules40. Structural and biochemical studies of ClpB showed that the coiled coils are arranged in an antiparallel orientation and are highly flexible40 as observed for the stalk coiled coil of dynein18. Moreover, a cross-linking study has revealed that mobility within the coiled coils is critical for ClpB functions, and disulfide cross-linking within the coiled coils affects its ATPase activity41, similar to the stalk coiled coil of dynein as shown in the present study. These characteristics suggest that dynein and the AAA+ protein(s) evolved from a common AAA+ ancestor containing a coiled-coil fold, and dynein adapted the mobility in its coiled coil to precisely couple ATPase steps and MT-binding activity for unidirectional movements along MT.

METHODS

Protein engineering, expression, and purification

We used here four types of the 380-kDa motor domain (V1383–I4725) of the *D. discoideum* cytoplasmic dynein heavy chain: HFG380, HFG380B2, HFG380P, and HFG380-SRS. Construction of expression plasmids for HFG380 and HFG380B2 has been described previously16,29. To construct HFG380P, two recognition sequences for PreScission protease, encoding GGGSLEVLFQGPGGG and TGGGSLEVLFQGPGGTG, were inserted at two positions within the HFG380 gene, corresponding to between E3203–A3204 and between K3928–K3929, respectively. In addition, three point mutations, C3711N, C3792L, and C3888A, were introduced in AAA5 to suppress an oxidation-induced intrinsic mobility shift of the 83-kDa stalk-containing fragment. To produce the HFG380-SRS fusion mutants +βCC, αCC, and −βCC, a DNA fragment encoding the coiled-coil region of seryl-tRNA synthetase (L30–A96)26 was PCR-amplified and inserted into the HFG380 gene in place of its MTBD coding region (A3357–P3491, L3361–P3491, and A3364–P3491 for +βCC, αCC, and −βCC, respectively). Point mutations to produce the single-and double-Cys mutants of HFG380, HFG380B2, and HFG380P were introduced using the QuikChange mutagenesis kit (Stratagene) according to the manufacturer's instructions. After verifying the DNA sequence of PCR-amplified or mutagenized regions, each expression plasmid was introduced into *D. discoideum* cells, and the expressed recombinant dynein motor domain was purified as described16. Protein concentrations were determined by the Bradford

method standardized with bovine serum albumin. MT concentration is expressed as the tubulin dimer concentration.

Oxidative disulfide cross-linking and reducing treatments

Treatments were performed in the presence of ~90 μM ATP as follows except the experiments shown in Figure 2d and Supplementary Figure 1b. Oxidation was performed using a Cu(II)-(1,10-phenanthroline)$_3$ complex prepared by mixing equal volumes of freshly prepared 180 mM phenanthroline (dissolved in ethanol) and aqueous 60 mM $CuSO_4$. This stock was diluted 1:10 with water just before use. Prior to oxidation, dynein (1–2 μM) was passed through a NAP-5 column to replace the solvent with PMEG30-EDTA buffer (30 mM K-PIPES, 4 mM $MgCl_2$, 5 mM EGTA, 0.9 M glycerol; pH 7.0) supplemented with 0.1 mM ATP. Oxidation used 300 μM copper-phenanthroline complex in ice, terminated after 5 min by 15 mM EDTA. The oxidized dynein was passed through a NAP-5 column to replace the solvent with a dynein assay buffer (10 mM K-PIPES, 50 mM potassium acetate, 4 mM $MgSO_4$, 1 mM EGTA; pH7.0) supplemented with 0.1 mM ATP. Reduction of disulfide bonds was by 10 mM TCEP-HCl at 4 °C for 12–16 h. For the experiments shown in Figure 2d and Supplementary Figure 1b, the double-Cys mutants in dynein assay buffer supplemented with 17.5 μM paclitaxel and 125 μM GTP were oxidized with 100 μM copper-phenanthroline complex at room temperature (~24 °C) in the presence of 1 mM ADP, 1 mM ATP plus 0.2 mM vanadate, or 1mM ADP plus 15 μM MT for the time indicated. The desalting step after oxidation was omitted.

Non-reducing SDS-PAGE and Western blotting analyses

Untreated, oxidized, and reduced HFG380P and its mutants were treated with ~100 units ml^{-1} PreScission protease (GE Healthcare) in dynein assay buffer supplemented with 0.1 mM ATP at 4 °C for 12–16 h. The sample was then mixed 1:1 with 2× sample buffer containing 25 mM N-ethylmaleimide and no reducing agent, incubated on ice for 10 min, boiled for 5 min, and stored at −30 °C. Samples were run on SDS-PAGE gel, transferred onto PVDF membrane, and probed with a rabbit antibody against the stalk region of *D. discoideum* cytoplasmic dynein heavy chain42. Blots were then incubated with horseradish peroxidase-conjugated goat anti-rabbit antibody, and the bands were visualized using an ECL plus system (GE Healthcare). The intensities of Coomassie-stained bands on SDS-PAGE gel were quantified using Image J 1.41o (NIH).

EM analysis

Oxidized double-Cys mutants of HFG380 were analyzed by negative-stain EM and single-particle image processing as described previously18,43. Briefly, oxidized dynein was diluted to ~40 nM with dynein assay buffer and negatively stained with 1% (w/v) uranyl acetate on carbon-coated grids that were freshly UV-treated. Micrographs were taken at 40,000× nominal magnification on a JEOL 1200 EX operating at 80 kV with a LaB_6 electron source. Magnification was calibrated using paramyosin filaments. Micrographs were digitized at 0.504 nm/pixel on an Imacon Flextight 848 scanner and processed using the SPIDER suite.

Measurements of ATPase and MT-binding activities

Basal and MT-activated ATPase rates of the dynein motor domain were measured in dynein assay buffer supplemented with 10 μM paclitaxel using a coupled enzymatic assay (EnzChek phosphate assay kit, Molecular Probes) in the presence of 1 mM ATP at 25 °C as described8,16, except that 2 mg ml^{-1} bovine serum albumin was added to the reaction mixture to stabilize dynein activity. Steady-state MT-binding was determined by cosedimentation in dynein assay buffer supplemented with 5 μM free paclitaxel and 250 μM GTP at 25 °C as described36. HFG380 or its mutant (50 nM) was mixed with various concentrations of paclitaxel-stabilized MT in the absence or presence of 3.3 mM ATP. After ~1-min incubation, the mixtures were centrifuged at 100,000*g* for 10 min. The concentration of HFG380 in the supernatants was determined using the fluorescence intensity of the GFP moiety (excitation at 488 nm, emission at 510 nm) with reference to that of known concentrations of HFG380.

Pre-steady-state fluorescence measurements

Pre-steady-state kinetic experiments were performed with an SX-18MV stopped-flow apparatus (Applied Photophysics) using dynein assay buffer supplemented with 0.1 mM ADP at 25 °C essentially as described previously30. Time courses of changes in the FRET signal were followed by exciting the donor (BFP) at 380 nm and monitoring the emission intensity of the accepter (GFP) with a 515-nm long-pass filter. The recovery-stroke transition was monitored after mixing 60 nM HFG380B2 or its mutants with 1 mM ATP. For observation of the powerstroke transition, a sequential mixing mode was used: 120 nM dynein and 50 μM ATP were first mixed to obtain the majority of the dynein in the pre-powerstroke state, then 50 mM glucose and excess hexokinase (2,000 units ml^{-1}) were added to the mixture after a delay of 98–102 ms to deplete free ATP. Higher concentrations of hexokinase (2,500–4,000 units ml^{-1}) yielded similar k_{obs} values, confirming that 2,000 units ml^{-1} hexokinase was sufficient. All concentrations given here are final after mixing.

Supplementary Material

Refer to Web version on PubMed Central for supplementary material.

ACKNOWLEDGMENTS

We thank Michael Koonce (Wadsworth Center) for generously providing the anti-stalk antibody. This work was supported by a Grant-in-Aid for Scientific Research (S) from the Japan Society for the Promotion of Science (JSPS) to K.S., a Grant-in-Aid for Scientific Research on Priority Areas from the Ministry of Education, Culture, Sports, Science, and Technology of Japan (MEXT) to K.S., a Grant-in-Aid for Young Scientists (A) from MEXT to T.K., and in part by The Wellcome Trust to A.J.R., the BBSRC (UK) to S.A.B. and P.J.K, and Grant GM30401 from the National Institutes of Health to I.R.G.

REFERENCES

1. Gibbons IR, Rowe AJ. Dynein: a protein with adenosine triphosphatase activity from cilia. Science. 1965; 149:424–426. [PubMed: 17809406]
2. Paschal BM, Vallee RB. Retrograde transport by the microtubule-associated protein MAP 1C. Nature. 1987; 330:181–183. [PubMed: 3670402]
3. DiBella LM, King SM. Dynein motors of the Chlamydomonas flagellum. Int. Rev. Cytol. 2001; 210:227–268. [PubMed: 11580207]

4. Vale RD. The molecular motor toolbox for intracellular transport. Cell. 2003; 112:467–480. [PubMed: 12600311]
5. Vallee RB, Williams JC, Varma D, Barnhart LE. Dynein: An ancient motor protein involved in multiple modes of transport. J. Neurobiol. 2004; 58:189–200. [PubMed: 14704951]
6. Pfister KK, et al. Genetic analysis of the cytoplasmic dynein subunit families. PLoS Genet. 2006; 2:e1. [PubMed: 16440056]
7. Neuwald AF, Aravind L, Spouge JL, Koonin EV. AAA+: A class of chaperone-like ATPases associated with the assembly, operation, and disassembly of protein complexes. Genome Res. 1999; 9:27–43. [PubMed: 9927482]
8. Nishiura M, et al. A single-headed recombinant fragment of Dictyostelium cytoplasmic dynein can drive the robust sliding of microtubules. J. Biol. Chem. 2004; 279:22799–22802. [PubMed: 15051717]
9. Reck-Peterson SL, et al. Single-molecule analysis of dynein processivity and stepping behavior. Cell. 2006; 126:335–348. [PubMed: 16873064]
10. Samso M, Radermacher M, Frank J, Koonce MP. Structural characterization of a dynein motor domain. J. Mol. Biol. 1998; 276:927–937. [PubMed: 9566197]
11. Ogura T, Wilkinson AJ. AAA+ superfamily ATPases: common structure--diverse function. Genes Cells. 2001; 6:575–597. [PubMed: 11473577]
12. Mocz G, Gibbons IR. Phase partition analysis of nucleotide binding to axonemal dynein. Biochemistry. 1996; 35:9204–9211. [PubMed: 8703926]
13. Gibbons IR, et al. Photosensitized cleavage of dynein heavy chains. Cleavage at the "V1 site" by irradiation at 365 nm in the presence of ATP and vanadate. J. Biol. Chem. 1987; 262:2780–2786. [PubMed: 2950090]
14. Silvanovich A, Li MG, Serr M, Mische S, Hays TS. The third P-loop domain in cytoplasmic dynein heavy chain is essential for dynein motor function and ATP-sensitive microtubule binding. Mol. Biol. Cell. 2003; 14:1355–1365. [PubMed: 12686593]
15. Reck-Peterson SL, Vale RD. Molecular dissection of the roles of nucleotide binding and hydrolysis in dynein's AAA domains in Saccharomyces cerevisiae. Proc. Natl. Acad. Sci. U S A. 2004; 101:1491–1495. [PubMed: 14755060]
16. Kon T, Nishiura M, Ohkura R, Toyoshima YY, Sutoh K. Distinct functions of nucleotide-binding/hydrolysis sites in the four AAA modules of cytoplasmic dynein. Biochemistry. 2004; 43:11266–11274. [PubMed: 15366936]
17. Goodenough U, Heuser J. Structural comparison of purified dynein proteins with in situ dynein arms. J. Mol. Biol. 1984; 180:1083–1118. [PubMed: 6241263]
18. Burgess SA, Walker ML, Sakakibara H, Knight PJ, Oiwa K. Dynein structure and power stroke. Nature. 2003; 421:715–718. [PubMed: 12610617]
19. King SM. The dynein microtubule motor. Biochim. Biophys. Acta. 2000; 1496:60–75. [PubMed: 10722877]
20. Gee MA, Heuser JE, Vallee RB. An extended microtubule-binding structure within the dynein motor domain. Nature. 1997; 390:636–639. [PubMed: 9403697]
21. Koonce MP. Identification of a microtubule-binding domain in a cytoplasmic dynein heavy chain. J. Biol. Chem. 1997; 272:19714–19718. [PubMed: 9242627]
22. Howard, J. Mechanics of Motor Proteins and the Cytoskeleton. Sinauer Associates, Massachusetts; 2001.
23. Schliwa M, Woehlke G. Molecular motors. Nature. 2003; 422:759–765. [PubMed: 12700770]
24. Vallee RB, Gee MA. Make room for dynein. Trends Cell Biol. 1998; 8:490–494. [PubMed: 9861671]
25. Oiwa K, Sakakibara H. Recent progress in dynein structure and mechanism. Curr. Opin. Cell Biol. 2005; 17:98–103. [PubMed: 15661525]
26. Gibbons IR, et al. The affinity of the dynein microtubule-binding domain is modulated by the conformation of its coiled-coil stalk. J. Biol. Chem. 2005; 280:23960–23965. [PubMed: 15826937]

27. Shimizu T, Johnson KA. Presteady state kinetic analysis of vanadate-induced inhibition of the dynein ATPase. J. Biol. Chem. 1983; 258:13833–13840. [PubMed: 6227617]
28. Shima T, Kon T, Imamula K, Ohkura R, Sutoh K. Two modes of microtubule sliding driven by cytoplasmic dynein. Proc. Natl. Acad. Sci. U S A. 2006; 103:17736–17740. [PubMed: 17085593]
29. Kon T, Mogami T, Ohkura R, Nishiura M, Sutoh K. ATP hydrolysis cycle-dependent tail motions in cytoplasmic dynein. Nat. Struct. Mol. Biol. 2005; 12:513–519. [PubMed: 15880123]
30. Mogami T, Kon T, Ito K, Sutoh K. Kinetic characterization of tail swing steps in the ATPase cycle of Dictyostelium cytoplasmic dynein. J. Biol. Chem. 2007; 282:21639–21644. [PubMed: 17548361]
31. Volkman BF, Lipson D, Wemmer DE, Kern D. Two-state allosteric behavior in a single-domain signaling protein. Science. 2001; 291:2429–2433. [PubMed: 11264542]
32. Arora K, Brooks CL 3rd. Large-scale allosteric conformational transitions of adenylate kinase appear to involve a population-shift mechanism. Proc. Natl. Acad. Sci. U S A. 2007; 104:18496–18501. [PubMed: 18000050]
33. Carter AP, et al. Structure and Functional Role of Dynein's Microtubule-Binding Domain. Science. 2008; 322:1691–1695. [PubMed: 19074350]
34. Holzbaur EL, Johnson KA. Microtubules accelerate ADP release by dynein. Biochemistry. 1989; 28:7010–7016. [PubMed: 2531005]
35. Holzbaur EL, Johnson KA. ADP release is rate limiting in steady-state turnover by the dynein adenosinetriphosphatase. Biochemistry. 1989; 28:5577–5585. [PubMed: 2528374]
36. Imamula K, Kon T, Ohkura R, Sutoh K. The coordination of cyclic microtubule association/dissociation and tail swing of cytoplasmic dynein. Proc. Natl. Acad. Sci. U S A. 2007; 104:16134–16139. [PubMed: 17911268]
37. Gennerich A, Carter AP, Reck-Peterson SL, Vale RD. Force-induced bidirectional stepping of cytoplasmic dynein. Cell. 2007; 131:952–965. [PubMed: 18045537]
38. Martin J, Gruber M, Lupas AN. Coiled coils meet the chaperone world. Trends Biochem. Sci. 2004; 29:455–458. [PubMed: 15337117]
39. Schumacher J, Joly N, Rappas M, Zhang X, Buck M. Structures and organisation of AAA+ enhancer binding proteins in transcriptional activation. J. Struct. Biol. 2006; 156:190–199. [PubMed: 16531068]
40. Lee S, et al. The structure of ClpB: a molecular chaperone that rescues proteins from an aggregated state. Cell. 2003; 115:229–240. [PubMed: 14567920]
41. Haslberger T, et al. M domains couple the ClpB threading motor with the DnaK chaperone activity. Mol. Cell. 2007; 25:247–260. [PubMed: 17244532]
42. Samso M, Koonce MP. 25 Angstrom resolution structure of a cytoplasmic dynein motor reveals a seven-member planar ring. J. Mol. Biol. 2004; 340:1059–1072. [PubMed: 15236967]
43. Burgess SA, Walker ML, Sakakibara H, Oiwa K, Knight PJ. The structure of dynein-c by negative stain electron microscopy. J. Struct. Biol. 2004; 146:205–216. [PubMed: 15037251]
44. Gee M, Vallee R. The role of the dynein stalk in cytoplasmic and flagellar motility. Eur. Biophys. J. 1998; 27:466–473. [PubMed: 9760728]

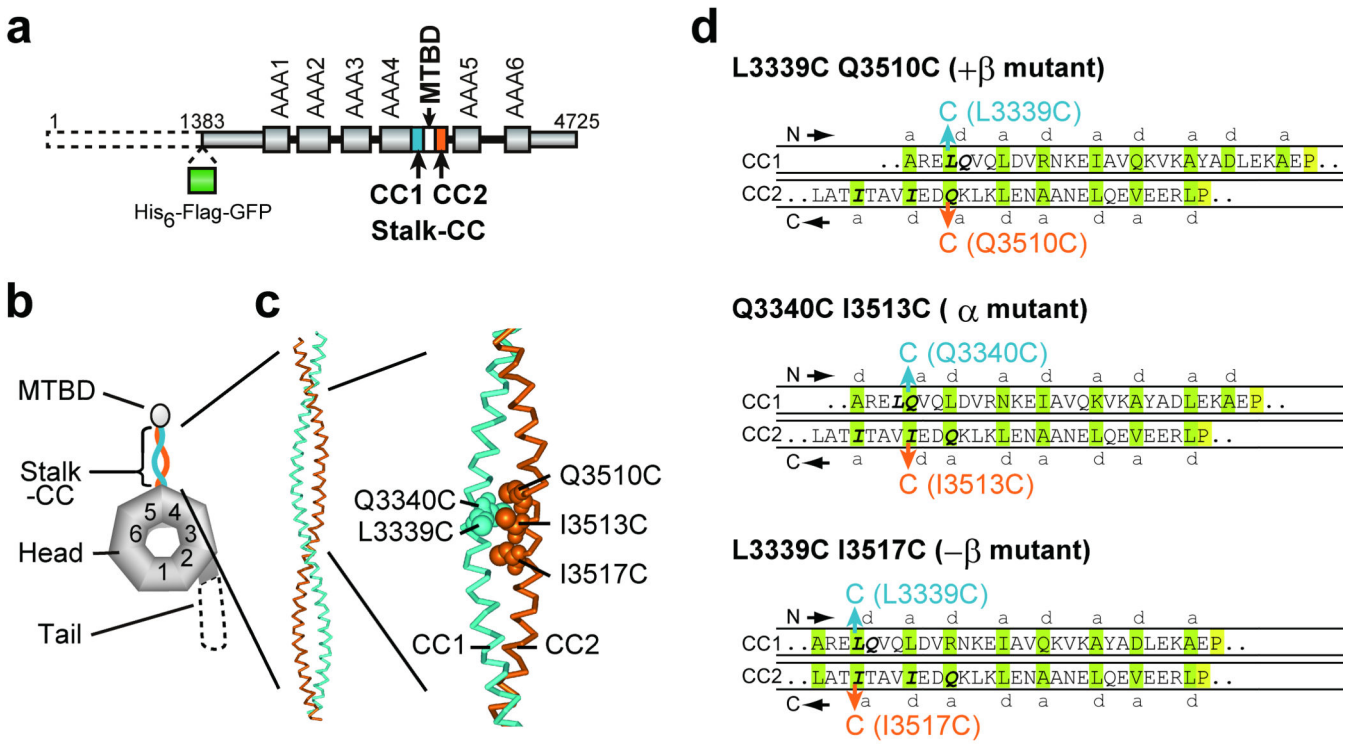

Figure 1.

Design of double-Cys mutants of the 380-kDa dynein motor domain for disulfide cross-linking between the two helices of the stalk coiled coil. (**a**) Domain organization and (**b**) predicted domain structure of the *D. discoideum* cytoplasmic dynein heavy chain. The dashed line represents the region deleted in the 380-kDa motor domain. (**c**) A homology-based structural model of the stalk coiled coil in the α registry (PDB id: 2bot26; numbered as in the *D. discoideum* dynein heavy chain) with Cys substitutions at L3339, Q3340, Q3510, I3513, and I3517 indicated by CPK representations. (**d**) Diagrams of the distal one-third portion of the stalk coiled coil that show expected alignments between the two helices in cross-linked double-Cys mutants. The introduced Cys pairs for disulfide bond formation are colored blue and orange. Amino acids predicted to occupy *a* and *d* positions of the heptad repeats 26 are shaded green. The absolutely conserved P3366 and P3491 residues, close to the boundary between the stalk and MTBD44, are shaded yellow. The +β, α, and −β registries correspond to the 26:19, 22:19, and 19:19 configurations, respectively, in ref. 26.

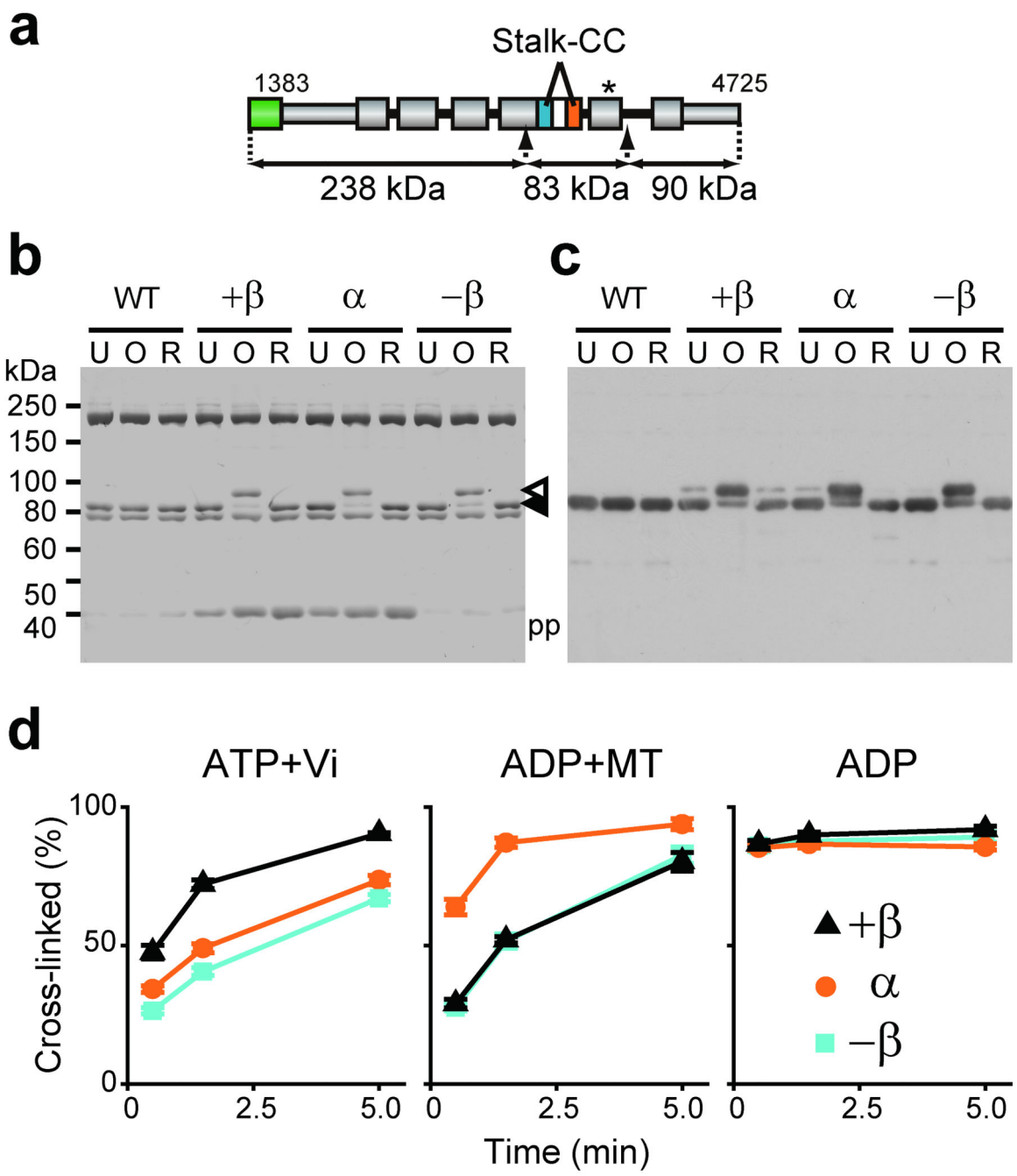

Figure 2.

Locking the registry between two helices of the stalk coiled coil of double-Cys mutants by oxidative disulfide cross-linking. (**a**) Diagram of HFG380P dynein. The arrows indicate insertion points of PreScission protease cleavage sites for excision of an 83-kDa stalk-containing fragment. The asterisk depicts three Cys substitutions, C3711N, C3792L, and C3888A introduced in AAA5 to suppress an oxidation-induced intrinsic mobility shift of the 83-kDa fragment. (**b** and **c**) Electrophoretic mobility shift assay of HFG380P (WT) and its double-Cys mutants. Dynein preparations were first untreated (U), oxidized for 5 min with

ATP present (O), or reduced after the oxidation (R), treated with protease, and finally analyzed by non-reducing SDS-PAGE with Coomassie Blue staining (**b**) and with immunoblotting using an anti-stalk antibody (**c**). The closed arrowhead indicates the un-cross-linked stalk, while the open arrowhead indicates an intramolecularly cross-linked stalk showing a decrease in electrophoretic mobility. pp indicates the PreScission protease. The ~200-kDa and ~75-kDa bands may correspond to the N-terminal and C-terminal fragments of HFG380P, respectively. (**d**) Effects of nucleotide/MT conditions on the disulfide cross-linking within the double-Cys mutants. Time courses of the disulfide bond formation in the presence of indicated nucleotide and/or MT were monitored by electrophoretic mobility shift assay as shown in Supplementary Figure 1b, and the percentage of cross-linked dynein was determined by densitometry. Values are displayed as the mean ± SD of six measurements using two independent dynein preparations.

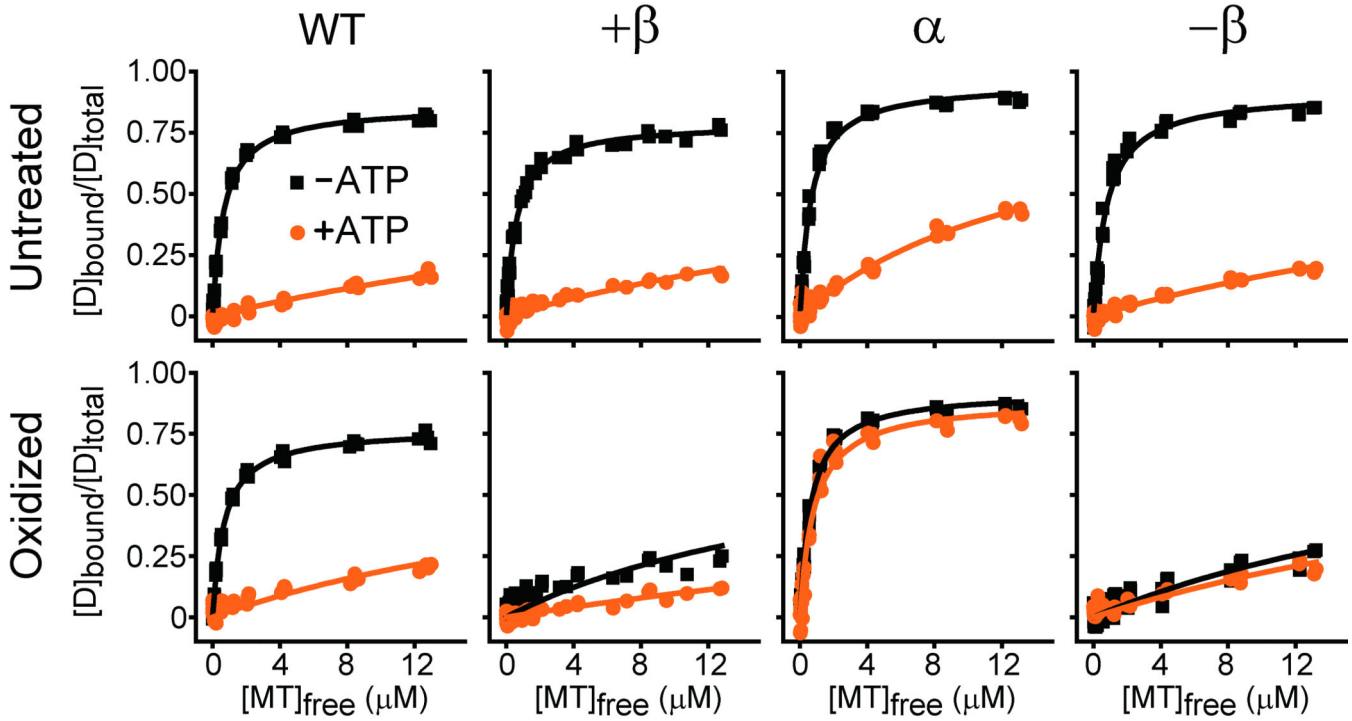

Figure 3.

Effects of locking the registry of the stalk coiled coil on ATP-sensitive MT-binding activity. HFG380 (WT) and its double-Cys mutants were untreated or oxidized, and then their MT-binding activities were measured by a cosedimentation assay with various concentrations of MT in the presence or absence of 3.3 mM ATP. Data were obtained using two independent dynein preparations. The smooth curves are the best fits of the data to hyperbolas with dissociation constant (K_d) and maximum binding (B_{max}) values given in Table 1.

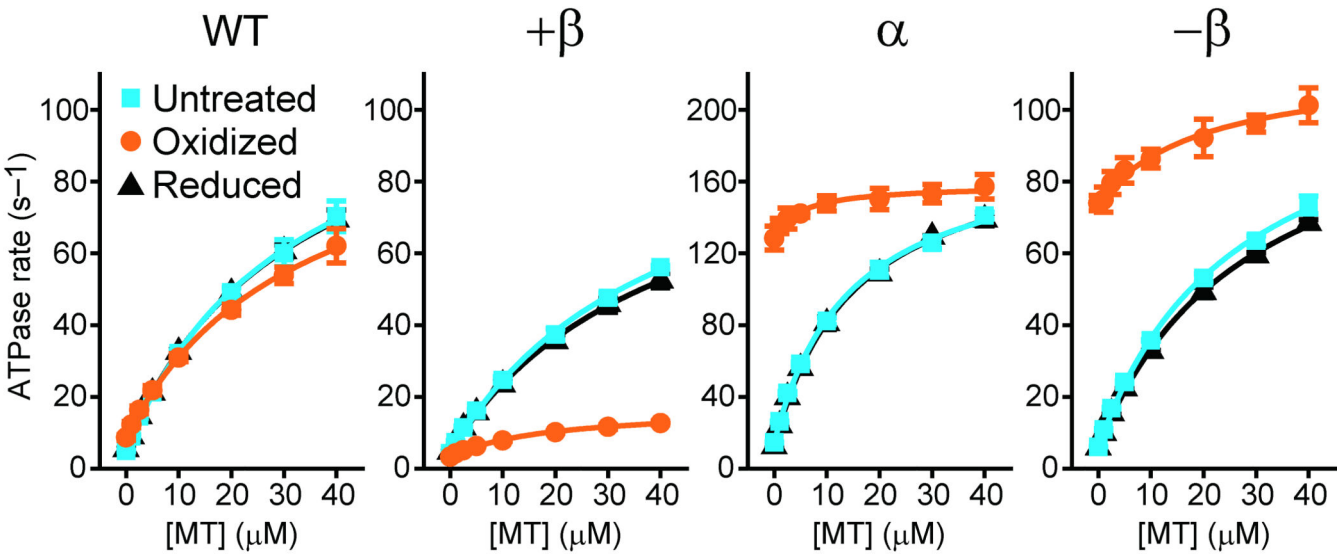

Figure 4.

Effects of locking the registry of the stalk coiled coil on MT-activated ATPase activity. HFG380 (WT) and its double-Cys mutants were untreated, oxidized, or reduced after the oxidation, and then their steady-state ATPase rates were measured as a function of MT concentration. Each symbol is the mean ± SD of at least three measurements using two independent dynein preparations. The smooth curves are the best fits of the data to the Michaelis-Menten equation with k_{cat} and K_m (MT) values given in Table 1.

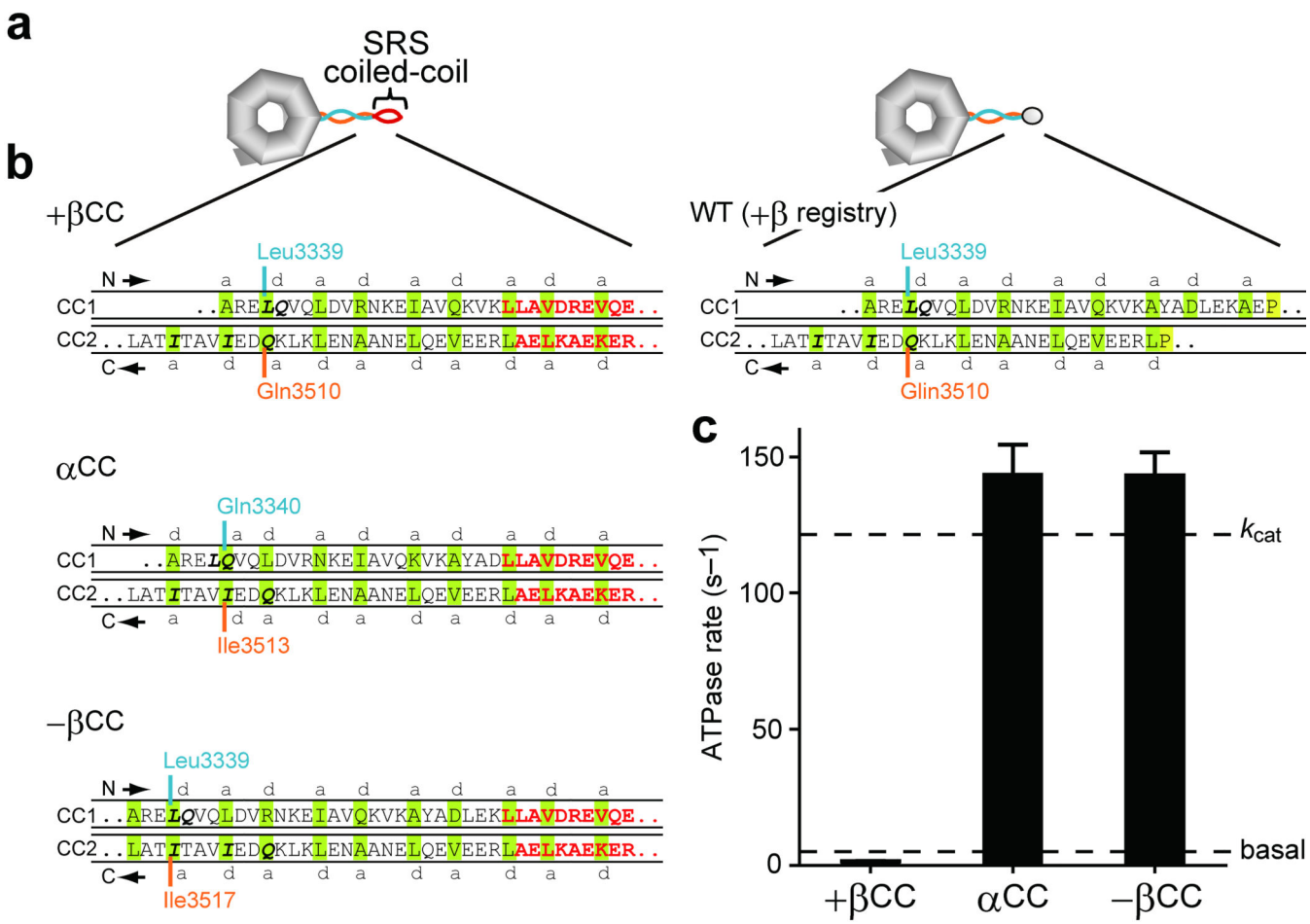

Figure 5.

Impact on dynein ATPase activity of fixing stalk registry using the stable antiparallel SRS coiled coil. (**a**) Scheme illustrating hypothetical structure of HFG380-SRS fusion mutants, +βCC, αCC, and −βCC, in which the MTBD of HFG380 was replaced by a stable antiparallel coiled coil from SRS26 for fixation of the registry of the stalk coiled coil near its distal end. (**b**) Diagrams showing expected alignments between the two helices of the stalk coiled coil in the HFG380-SRS fusion mutants. The diagrams depict the junctional region between the stalk coiled coil and the coiled coil from SRS. SRS-derived residues are colored red; amino acids predicted to occupy *a* and *d* positions of the heptad repeats26 are shaded green; the absolutely conserved P3366 and P3491 residues, close to the boundary between the stalk coiled coil and MTBD44, are shaded yellow. (**c**) ATPase activity of the HFG380-SRS fusion mutants. Values are displayed as the mean ± SD of six measurements using two independent dynein preparations. Dashed lines indicate the basal and k_{cat} values of wild-type HFG380.

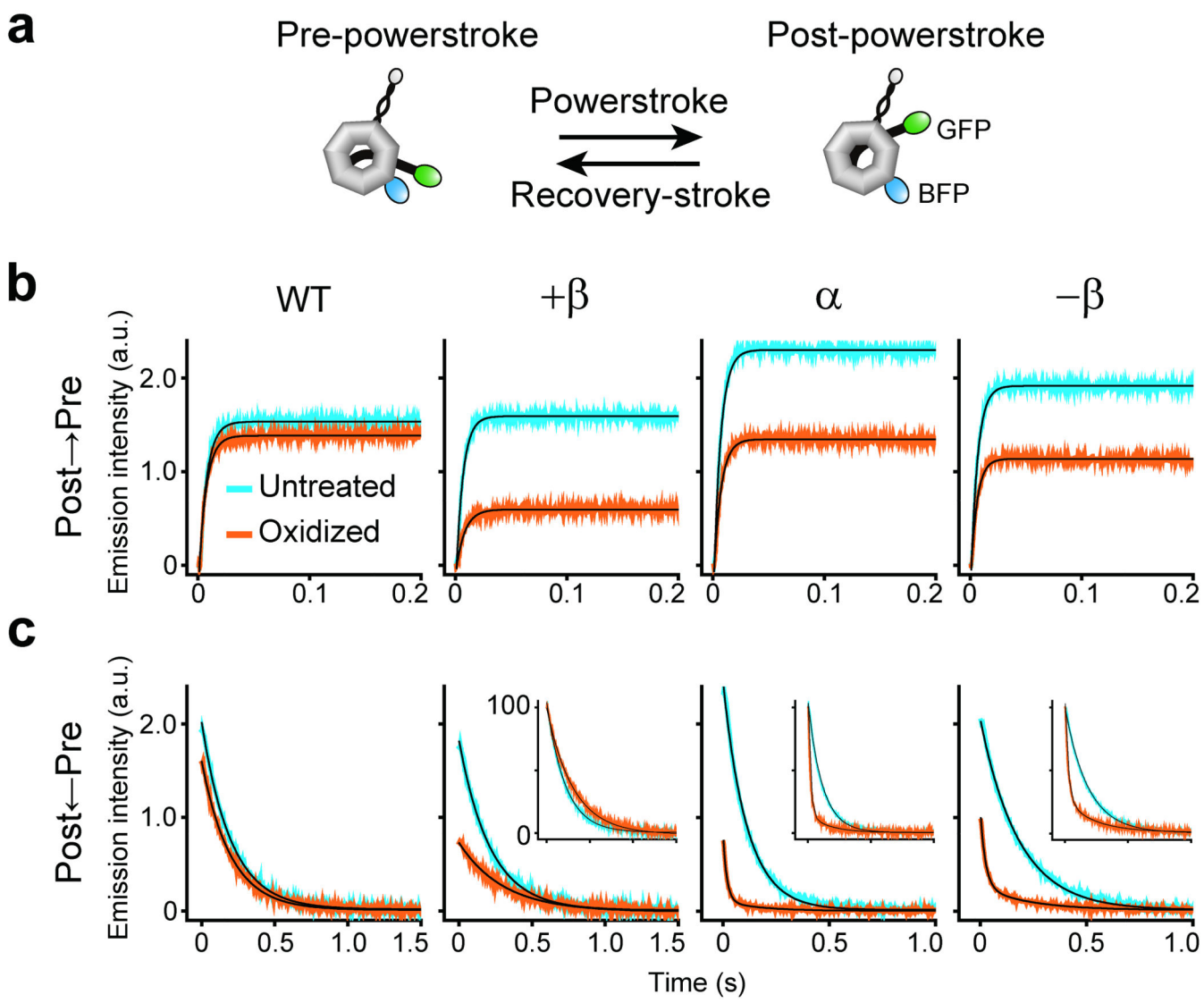

Figure 6.

Effects of locking the registry of the stalk coiled coil on the recovery-stroke and powerstroke steps in the mechanochemical cycle. (**a**) A scheme illustrating hypothetical structures of the dynein motor domain (HFG380B2) adopting either the pre-powerstroke or post-powerstroke conformation. (**b** and **c**) Representative time courses of the recovery-stroke transition (**b**) and the powerstroke transition (**c**), as monitored by changes in FRET-induced GFP fluorescence of HFG380B2 (WT) and its double-Cys mutants. The recovery-stroke transition was monitored upon mixing with excess ATP, while the powerstroke transition was observed just after mixing with hexokinase plus glucose to deplete free ATP. Each time course is the average of four to ten individual traces. The black curves are the best fits to double exponentials (for the powerstroke transition in oxidized α and −β mutants) or single exponentials (for the other cases); the mean apparent rate constants based on three measurements are given in Table 1. The insets show time courses with normalized amplitudes of the changes in GFP fluorescence.

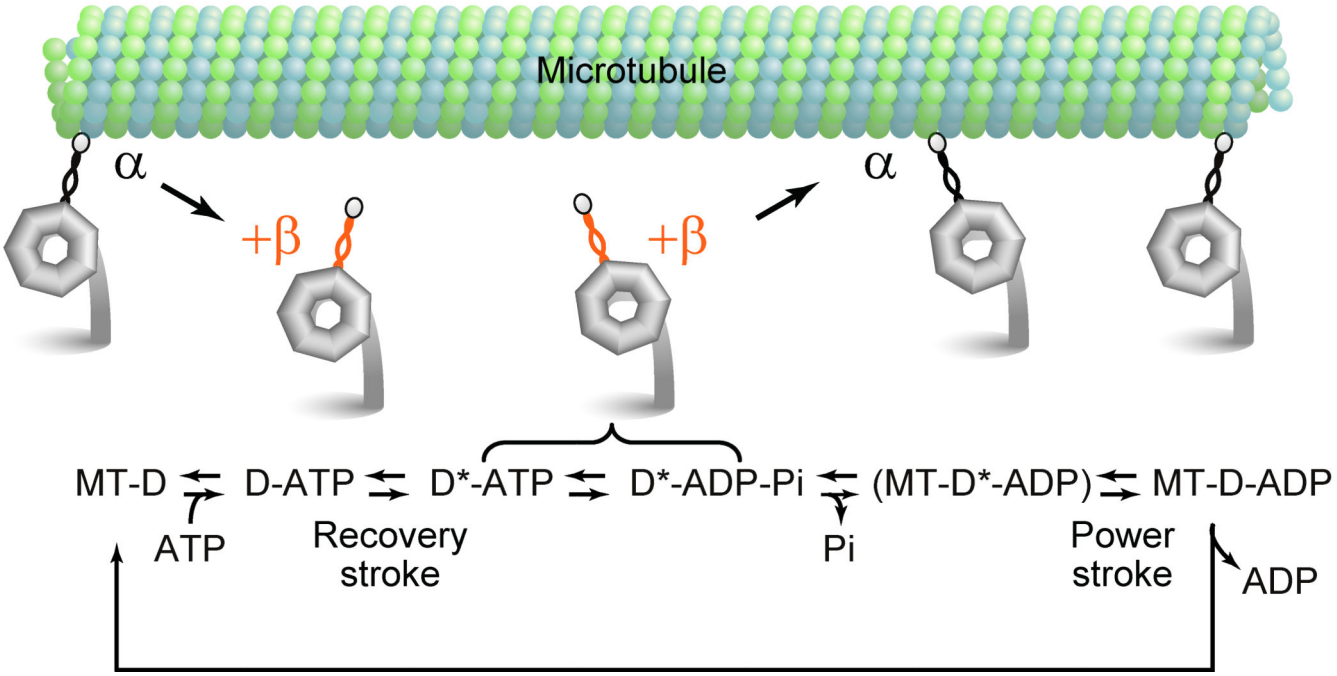

Figure 7.

Model for stalk-mediated two-way communication during the course of cytoplasmic dynein's mechanochemical cycle. The cartoon shows key steps in the mechanochemical cycle of a single-headed cytoplasmic dynein. The stalk coiled coil in the α and +β registries are colored black and orange, respectively. A scheme under the cartoon shows the ATPase cycle of cytoplasmic dynein. Here, D and D* represent dynein in the post-powerstroke and pre-powerstroke conformations, respectively. Communication between the ATP-hydrolyzing head and the MTBD is required in at least two different stages: ATP binding-induced dissociation of dynein from MT and MT binding-induced activation of a product releasing step. We propose that the former process is communicated by a structural change in the stalk coiled coil from the α to the +β registry, whereas the latter is transmitted by that from the +β to the α registry. For more details, see Discussion.

Nat Struct Mol Biol. Author manuscript; available in PMC 2009 October 05.

Table 1

Biochemical properties of the double-Cys mutants

Dynein		MT-activated ATPase			MT binding				Tail motions*	
		basal (s^{-1})	k_{cat} (s^{-1})	K_m(MT) (μM)	K_d (μM)		B_{max}		k_{obs}(post-pre) (s^{-1})	k_{obs}(pre-post) (s^{-1})
					−ATP	+ATP	−ATP	+ATP		
wild type HFG380	U	4.9 ± 0.1	121.1 ± 4.9	32.1 ± 2.5	0.66 ± 0.03	>10	0.86 ± 0.01	n/m	139.7 ± 8.4	4.9 ± 0.1
	O	8.7 ± 0.8	105.2 ± 4.2	33.3 ± 2.6	0.69 ± 0.02	>10	0.77 ± 0.01	n/m	155.1 ± 7.9	5.1 ± 0.1
	R	5.4 ± 0.2	120.0 ± 2.7	32.1 ± 1.4	–	–	–	–	–	–
+β (L3339C Q3510C)	U	4.2 ± 0.3	107.1 ± 6.0	40.5 ± 4.0	0.61 ± 0.03	>10	0.79 ± 0.01	n/m	161.7 ± 2.5	4.6 ± 0.1
	O	3.3 ± 0.1	17.0 ± 0.6	19.2 ± 1.7	>10	>10	n/m	n/m	123.4 ± 4.2	3.2 ± 0.0
	R	4.6 ± 0.2	100.4 ± 5.2	40.4 ± 3.7	–	–	–	–	–	–
α (Q3340C I3513C)	U	14.5 ± 0.2	182.8 ± 4.8	14.5 ± 1.0	0.65 ± 0.04	>10	0.96 ± 0.01	n/m	156.3 ± 2.7	9.4 ± 0.4
	O	128.4 ± 6.6	158.0 ± 1.7	5.0 ± 1.0	0.65 ± 0.03	0.85 ± 0.09	0.92 ± 0.01	0.89 ± 0.02	154.5 ± 3.5	47.5 ± 5.3**
	R	12.3 ± 0.6	185.3 ± 4.1	15.0 ± 0.9	–	–	–	–	–	–
−β (L3339C I3517C)	U	6.0 ± 0.1	116.4 ± 4.4	26.6 ± 2.1	0.80 ± 0.07	>10	0.92 ± 0.02	n/m	162.8 ± 3.6	5.4 ± 0.1
	O	74.0 ± 2.1	112.9 ± 4.1	20.4 ± 4.6	>10	>10	n/m	n/m	185.4 ± 6.8	41.5 ± 1.3**
	R	5.8 ± 0.3	112.0 ± 3.7	28.7 ± 1.9	–	–	–	–	–	–

U, untreated; O, oxidized; R, reduced after the oxidation; B_{max}, maximum binding; –, not tested; n/m, not measurable;

* the values were obtained from HFG380B2-based constructs;

** the values are those for the major fast component (~80% in amplitude) of the double-exponential fits.